Lipid Nanotube Formation Using Space-Regulated Electric Field above Interdigitated Electrodes

Hongmei Bi, Dingguo Fu, Lei Wang, and Xiaojun Han*

State Key Laboratory of Urban Water Resource and Environment, School of Chemical Engineering and Technology, Harbin Institute of Technology, Harbin 150001, China

ABSTRACT Lipid nanotubes have great potential in biology and nanotechnology. Here we demonstrate a method to form lipid nanotubes using space-regulated AC electric fields above coplanar interdigitated electrodes. The AC electric field distribution can be regulated by solution height above the electrodes. The ratio of field component in *x* axis (Ex) to field component in *z* axis (Ez) increases dramatically at solution height below 50 μm; therefore, at lower solution height, the force from Ex predominantly drives lipids to form lipid nanotubes along with the electric field direction. The forces exerted on the lipid nanotube during its formation were analyzed in detail, and an equation was obtained to describe the relationship among nanotube length and field frequency, amplitude, and time. We believe that the presented approach opens a way to design and prepare nanoscale materials with unique structural and functional properties using space-regulated electric fields.

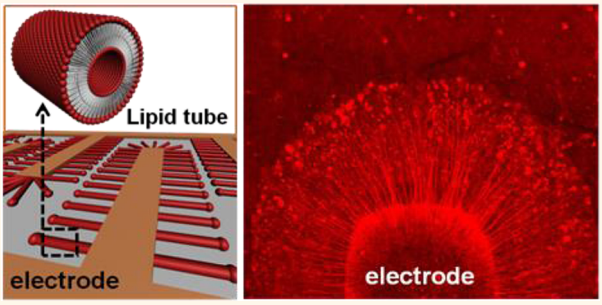

KEYWORDS: lipid nanotube · Interdigitated electrodes · AC electric field · finite element analysis · FRAP

Lipid nanotubes, the self-assembled hollow cylindrical tubule of lipid molecules, are widespread in nature. As an important existence form of phospholipids, they play an important role in intracellular transport phenomena.[1,2] The transport of ions and proteins through them has been monitored in a diverse range of cells, including lymphocytes, macrophages, adrenal cells, and cardiomyocytes.[3−5] The fabrication of lipid nanotubes *in vitro* has been an exciting research topic because of its interesting applications not only in biology but also in nanotechnology. Lipid nanotubes were used as microreactors for nanorod or nanowire formation,[6−8] templates for fabricating nanowires by metallization on their surfaces,[9−12] and carriers for embedding of nanoparticles inside lipid bilayers.[13−15] A number of fabrication techniques have been developed after the first lipid nanotube was artificially created more than three decades ago.[16] These fabrication methods can be roughly categorized into two classes: self-assembly of lipid molecules and stretching lipid aggregates using external forces. Lipid nanotubes were made by self-assembly of 1,2-bis(10,12-tricosadiynoyl)-*sn*-glycero-3-phosphocholine ($DC_{8,9}PC$) by mixing lipid alcoholic solution with water in varying proportions.[17,18] The conversion efficiency of tubular microstructures was improved by changing the experimental parameters.[18,19] Other nucleobase-derived amphiphiles mixed with phospholipids were also reported to self-assemble into lipid tubes.[20,21] The self-assembly method is limited to special lipid mixtures. As to the approach of stretching lipid aggregates using external forces, lipid nanotubes were fabricated by exerting external microfluidic shear force on lipid aggregates,[22−24] as well as by pulling lipid vesicles with a pipet,[1,25] a microneedle,[26] or an optical tweezer,[27] which require complicated equipment.

Nonuniform AC electric fields were exploited for controlling the motion, separation, and assembly of nanomaterials depending on their dielectric properties.[28−30] In biochemistry or the field of medicine, AC electric fields were widely applied to prepare giant unilaminar vesicles.[31−33] However, to the best of our knowledge, there are no reports on exploring AC electric fields for the fabrication of lipid nanotubes. Herein we found that the

* Address correspondence to hanxiaojun@hit.edu.cn.

Received for review February 13, 2014 and accepted March 26, 2014.

Published online March 26, 2014
10.1021/nn500876z

field distribution in aqueous solution above coplanar interdigitated electrodes can be regulated by the distance between electrode and top insulator (*i.e.*, solution height). At higher solution height, the lipid vesicles were produced, while at enough low aqueous solution height, lipid nanotubes were generated by the AC electric field of a coplanar interdigitated electrode system. We control the electric field distribution between interdigitated electrodes by varying solution height and found that the ratio of lateral field component to vertical field component played an important role in forming lipid nanotubes. Detailed numerical analysis has been done to understand this phenomenon. Theoretical values are consistent with experimental results. The possible mechanism of lipid nanotube formation was proposed. The formed nanotube was used as a template for mineralization of silica film for further bioapplications. It opens a way to design and prepare new nanoscale materials with unique structural and functional properties using space-regulated electric fields.

RESULTS AND DISCUSSION

Formation of Lipid Nanotubes Using Interdigitated Indium Tin Oxide (ITO) Electrodes. The interdigitated ITO electrodes (200 μm in width, 160 nm in thickness) coated with thin lipid films and a coverslip were separated by a rectangular plastic frame, as shown in Figure 1a. The frame acts as a spacer to control the solution height above the electrodes. Two electrode pads were firmly connected to a signal generator (TTi, TGA12104, England) to apply the AC electric field to induce lipid nanotube formation. Figure 1b is the schematic drawing of lipid nanotubes formed on electrodes (oblique view). A 3D structure of lipid nanotubes is also illustrated in Figure 1b. Using this setup, lipid nanotubes were generated with a 20 μm thick spacer as shown in Figure 1c–e. Figure 1c is a typical fluorescence image of L-α-phosphatidylcholine (egg PC) nanotubes containing 0.5% Texas red-labeled 1,2-dihexadecanoyl-*sn*-glycero-3-phosphoethanolamine, triethylammonium salt (TR-DHPE) formed at the tip of an electrode at a field of 5 V, 10 Hz for 25 min, while Figure 1d is a high-magnification fluorescence image of lipid nanotubes under the same experimental conditions. Figure 1e is a fluorescence image of 1,2-dioleoyl-*sn*-glycero-3-phosphocholine (DOPC) nanotubes labeled with 0.5% TR-DHPE formed between two neighboring electrodes. Lipid nanotubes radially grew toward the solution, like a crown, at the tip of the electrode with same length, and grew vertically to the electrode edge between two neighboring electrodes. Except for pure egg PC or DOPC lipid, egg PC mixed with cholesterol (mass ratio of 10:1) and DOPC mixed with cholesterol (mass ratio of 5:1) also formed lipid nanotubes using this method. Therefore, this method has a certain degree of universality. The diameter of the nanotube

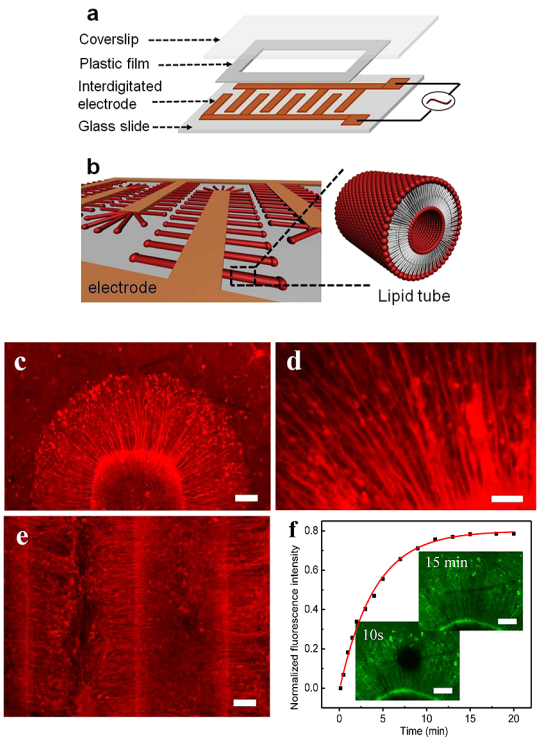

Figure 1. Schematic of lipid nanotube electroformation setup and fluorescence images of the formed lipid nanotubes. (a) Schematic drawing of lipid nanotube electroformation setup, which contains an interdigitated ITO electrode (bottom) and a glass coverslip (top) separated by a rectangular plastic frame. Not to scale. (b) Schematic illustration of lipid nanotube formed on electrodes (oblique view). The zoom-in view is the 3D structure of a lipid nanotube. (c) Low-magnification and (d) high-magnification fluorescence images of egg PC (doped with 0.5% TR-DHPE) lipid nanotubes at the tip of the electrode under an AC field of 5 V and 10 Hz with a solution height of 20 μm. (e) DOPC (doped with 0.5% TR-DHPE) lipid nanotubes formed between two neighboring electrodes. (f) FRAP experiment of the lipid nanotube formed with an AC electric field. Fluorescent images of egg PC (doped with 2% 1,2-dioleoyl-*sn*-glycero-3-phosphoethanolamine-*N*-(7-nitro-2-1,3-benzoxadiazol-4-yl (NBD PE)) nanotubes were taken at 10 s and 15 min after photobleaching, respectively. The scale bars are (c,e,f) 50 μm and (d) 10 μm.

was measured to be in the range of 300–800 nm, which is similar to that in previous reports.[34,35] The diameter of the lipid nanotube is also consistent with theoretical value. Considering the physical properties of lipids,[22,36,37] the total free energy of the lamellar phase (E_L) and bilayer nanotube phase (E_T) can be expressed as

$$E_L = \left[\frac{k_c}{2}\left(\frac{1}{R_0}\right)^2 - W\right]A \quad (1)$$

$$E_T = \frac{k_c}{2}\left[\left(\frac{1}{R_{opt}}\right)^2 + \left(\frac{1}{R_0}\right)^2\right]A \quad (2)$$

$$A = 2\pi R_{opt} L \quad (3)$$

where R_0 represents the radius of spontaneous curvature of lipid membranes, k_c (74.5 pN nm, calculated value

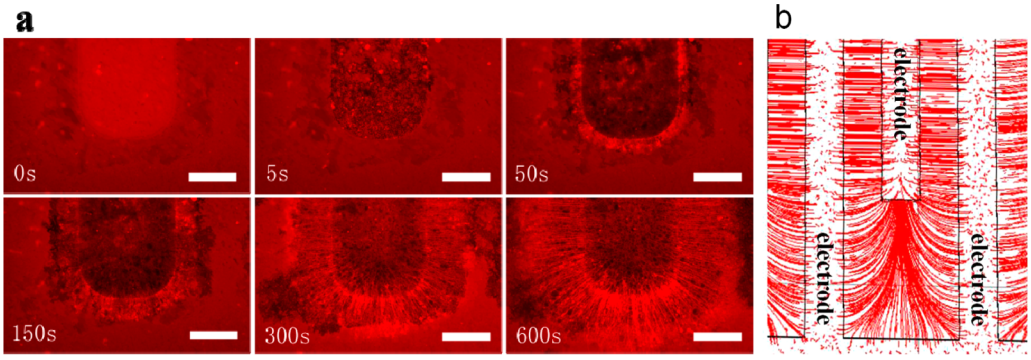

Figure 2. Growth in real time of lipid nanotubes and the simulated electric field lines. (a) Fluorescent images of lipid nanotube growth as a function of time (0, 5, 50, 150, 300, and 600 s) after applying AC electric field with amplitude of 5 V and frequency of 10 Hz with solution height of 20 μm. The scale bar is 100 μm. (b) Top view of simulated electric field lines generated at the same parameters as those in (a).

according to Table 1 in ref 36) is bending modulus, W (5.3×10^{-4} pN nm^{-1}, calculated value according to Table 1 in ref 36 and eqs 2, 13, 22, and 23 in ref 37) is interstitial energy, R_{opt} is the radius of the lipid nanotube, and L is the length of the lipid nanotube. Therefore, the energy required to form a nanotube is given below:

$$E_T - E_L = \frac{k_c}{2}\left[\left(\frac{1}{R_{opt}}\right)^2 + \left(\frac{1}{R_0}\right)^2\right]A - \left[\frac{k_c}{2}\left(\frac{1}{R_0}\right)^2 - W\right]A = \frac{k_c \pi L}{R_{opt}} + 2\pi R_{opt} WL \quad (4)$$

In the case of minimum energy ($E_T = E_L$), the nanotube radius (R_{opt}) is obtained: $R_{opt} = (k_c/2W)^{1/2} =$ 265 nm. The internal molecular mobility and stability of lipid nanotubes were investigated, as well. The diffusion coefficient of lipids in the nanotube were estimated to be $D = 2.73\ \mu m^2\ s^{-1}$ using the fluorescence recovery after photobleaching (FRAP) technique (Figure 1f).[38] This value is identical to that of a lipid bilayer on the glass surface.[39,40] The pH stability of egg PC lipid nanotubes is in the range from 3 to 8. Under the optimal pH of 7, lipid nanotubes can survive about 4 weeks at room temperature. In addition, the morphology and mobility of egg PC nanotubes are well maintained at 70 °C for 20 min.

Growth of Lipid Nanotubes in Real Time and Finite Element Analysis of Electric Field Distribution. The growth of lipid nanotubes was investigated by a microscope in real time at an amplitude of 5 V, frequency of 10 Hz, and solution height of 20 μm, as shown in Figure 2a. The fluorescent images were taken at 0, 5, 50, 150, 300, and 600 s after switching on the AC field. Just after applying a sinusoidal AC electric field, the initial calm ITO regions became drastically agitated immediately (image 5s in Figure 2a). The sprouts of lipid nanotubes were observed at the edge of the electrode after 20−50 s. Subsequently, the lipid nanotubes grew continuously from the electrode edge to the solution (images 150−600s in Figure 2a). From the finite element analysis of the electric field (Figure 2b) generated by 200 μm wide interdigitated electrodes using COMSOL software at same experimental conditions, it is noted that lipid nanotubes grow exactly along the electric field line direction.

Aforementioned results were obtained at a solution height of 20 μm. We found that the vesicles rather than lipid nanotubes were generated when solution height is over 100 μm (Supporting Information Figure S1). In order to understand the role of solution height in the electroformation of lipid nanotubes, we did finite element analysis of electric fields generated by 200 μm wide interdigitated electrodes at different solution heights at given amplitude of 5 V and frequency of 10 Hz. Simulation results of the electric field are shown in Figure 3a,b, which represent the field strength component in x axis (Ex, vertical to electrode edge, as indicated in the inset of Figure 3a) and z axis (Ez, vertical to electrode surface, as indicated in the inset of Figure 3b) at 20, 50, and 100 μm solution height. Display windows were selected from an electrode center to its neighbor electrode center. Ex mainly exists at the interval section of electrodes (Figure 3a), while Ez mainly centralizes on the top of the electrode section (Figure 3b). From the color change, it is noted that Ex varies more obviously than Ez with decreasing solution height. Therefore, solution height does influence the field distribution generated by coplanar interdigitated electrodes, especially for the Ex component.

The field strength of the cross section at 3 μm above the electrode surface from the simulation was analyzed quantitatively (Figure 3c,d). Ex increases gradually from the center of the electrodes and reaches the maximum at the edge of the electrodes, then maintains the greater strength at the interval section for each solution height (Figure 3c), while Ez almost remains constant in the electrode part and drops to approximately 0 at the interval between the electrodes (Figure 3d). Furthermore, Ex increases dramatically with decreasing solution height from 1466 V m^{-1} at 100 μm to 10700 V m^{-1} at 10 μm (Figure 3c). On the contrary,

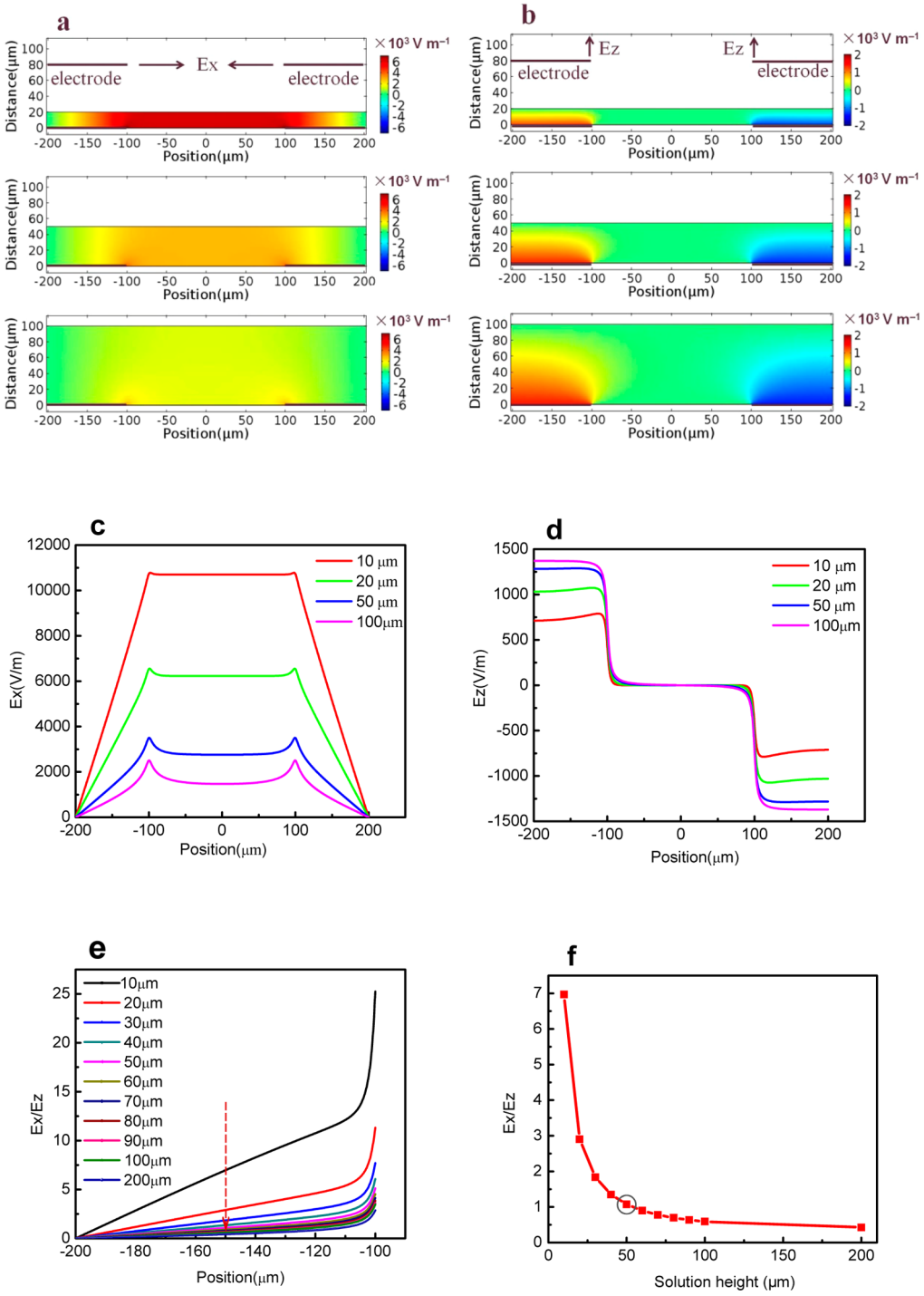

Figure 3. Simulated electric field generated by 200 μm width interdigitated electrodes at an amplitude of 5 V and a frequency of 10 Hz at varying solution height. (a,b) Color maps of the electric field component in *x* axis (Ex) and *z* axis (Ez) at 20, 50, and 100 μm solution height. (c,d) Curves of Ex and Ez components of electric field extracted from simulations at 3 μm cross section above the electrode surface at 10, 20, 50, and 100 μm solution height. (e) Ex/Ez data at different solution height at 3 μm cross section above the electrode surface from the center to the edge of one electrode. (f) Ex/Ez data as a function of solution height in the dotted line position in panel e.

Ez decreases with decreasing solution height (Figure 3d). Smaller solution height generates a stronger lateral electric field component, which is necessary for lipid nanotube growth. Conversely, it is easier to form vesicles at greater solution height because of the stronger vertical electric field component Ez. The critical solution height, deciding nanotube or vesicle formation using this system, is an important issue to be addressed afterward. So a series of simulation results of Ex/Ez in different solution heights were analyzed (Figure 3e). Figure 3f is the Ex/Ez at different solution heights at the same electrode position (dotted line in Figure 3e). It can be noted from Figure 3f

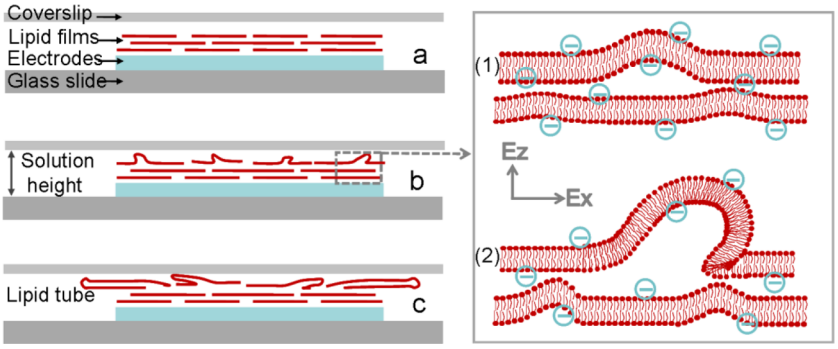

Figure 4. Schematic illustration of lipid nanotube formation mechanism. (a) Lipid film on the electrode surface without an AC electric field. (b) Sprout of lipid nanotube formation in the electroformation process. In the right box, step 1 is the bilayer vibration and separation under the effect of Ez mainly, while step 2 shows the pulling effect by Ex. (c) Lipid nanotube growth in the solution driven by Ex.

that Ex/Ez increases with decreasing solution height, which implies that Ex becomes more and more predominant. Ex/Ez decreases quickly less than 50 μm and then decreases gently when solution height is greater than 50 μm. We also did the same analysis at different electrode positions and found ~50 μm is the Ex/Ez changing transition area. Therefore, we propose that ~50 μm is the threshold solution height for lipid nanotube or vesicle formation using this method. In fact, the experimental results show that, in the case of 40−60 μm solution height, both lipid nanotubes and vesicles were generated. When the solution height is less than 40 μm, lipid nanotubes are the main products, while lipid vesicles are the main products at the solution height over 60 μm. Both experimental and simulated results demonstrate that the generation of lipid nanotubes is mainly dependent on the lateral field component of the applied AC electric field which can be regulated by solution height easily.

In order to investigate the effect of electrode thickness on lipid nanotube formation, a series of simulations were done at the electrode thicknesses of 1, 10, 50, 100, and 200 μm, while the solution height above the electrode top surface was fixed at 20 μm. Take a 200 μm thick electrode as an example; the field distributions of Ex and Ez are shown in Figure S2a,b, respectively. To make it more quantitative, the Ex/Ez of the cross section at 3 μm above the electrode surface was analyzed and presented in Figure S2c. The results show that there is no significant change of electric field distribution with various thicknesses of electrodes. Ex/Ez is independent of the electrode thickness above the main body of the electrode but becomes larger at the edge of the electrode surface with increasing electrode thickness, which is favorable for lipid nanotube formation. Therefore, the thickness of the electrodes does not affect the lipid nanotube formation above the electrode surface. Meanwhile, the space between two neighboring electrodes becomes greater with increasing electrode thickness. For the thicker electrode, the field between the side walls of two neighboring electrodes is similar to that generated by two face-to-face parallel electrodes, where Ex is responsible for vesicle formation and Ez generates the driving force for lipid nanotube formation. For 200 μm thick electrodes, by analyzing the Ez/Ex value of the cross section at 3 μm away from the electrode side wall (Figure S2d), it can be noted that the Ex component dominates in the lower part of the space between two neighboring electrodes, which enables lipid vesicle formation if the lipid films were distributed evenly on the side wall of the electrodes. Thus, the thick electrodes generate lipid nanotubes on the surface of the electrode and lipid vesicles between the electrodes. With decreasing electrode thickness, lipid nanotubes become the main products.

Possible Mechanism of Lipid Nanotube Electroformation. Combining our experimental results and the simulation data, we believe that the special electric field distribution at certain solution heights in this coplanar interdigitated electrode system is the intrinsic cause for lipid nanotube electroformation. The possible mechanism of this electroformation can be illustrated as Figure 4. Basically, it is a three-step process, that is, forming the lipid bilayer swells on the electrode surface, moving them to the edge of electrode, and pulling them into lipid nanotubes. At stage one, vertical electric field component Ez plays an important role, which induces lipid bilayer separation to form swells (step 1 in Figure 4b). The higher electric density induced by the electric field leads to the smaller surface tension on the lipid film, which is conducive to form tubular buds with smaller diameter. At stage two, lateral electric field force from Ex pulls the tubular bud to the edge of the electrode (step 2 in Figure 4b). The formation and moving of the lipid nanotube sprout was observed within a minute (Figure 2a). At the final stage, when the sprouts of lipid nanotubes shift to the border of the electrode, the electric field force from Ex becomes the main driving force of nanotube growth, which is confirmed by the observation of the pulsation of lipid nanotube growth at a

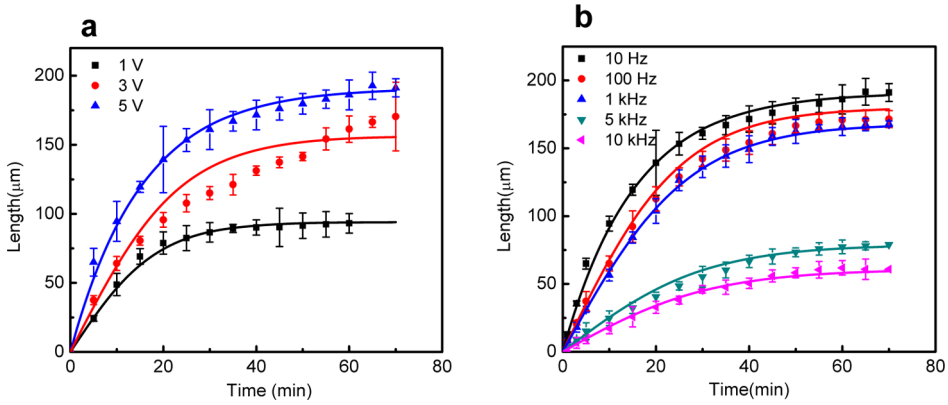

Figure 5. Lipid nanotube length against time and fitting curves under different AC electric fields. (a) Scatter diagram and fitting curve of lipid nanotube length against time at amplitudes of 1 (black), 3 (red), and 5 V (blue) at a frequency of 10 Hz. (b) Scatter diagram and fitting curve of lipid nanotube growth length at frequencies of 10 Hz (black), 100 Hz (red), 1 kHz (blue), 5 kHz (green), and 10 kHz (pink) at an amplitude of 5 V. Solid lines are all the corresponding fitting curves using eq 7.

frequency of 1 Hz (Supporting Information movie S1). The succedent noncompact lipid film continues to bulge, elongate, and grow along with the original sprout of the lipid nanotube as the cylinder nanotubes are driven by Ex (Figure 4c). The elastic force will increase with the increasing length of lipid nanotube, which is the obstruction for the lipid growth. When this driving force is equal to the sum of bending force and resilience, the lipid nanotube stops growing and reaches its maximum length. Similar to electroformed giant unilamellar vesicles, the lipid nanotubes formed in this way are probably unilamellar.

Lipid Nanotube Formation Influenced by AC Electric Field Parameters. There are obviously two other extrinsic parameters influencing the formation of lipid nanotube (*i.e.*, amplitude and frequency of applied AC electric field). In the following contents, the influences of amplitude and frequency on egg PC lipid nanotube formation were studied in detail when the temperature and solution height were kept at 26 °C and 20 μm, respectively. The real-time measurement of lipid nanotube length under different amplitudes and frequencies were measured and plotted in Figure 5. Scatter dots are experimental results at amplitudes of 1 (black), 3 (red), and 5 V (blue) with a frequency of 10 Hz (Figure 5a) and at frequencies of 10 Hz (black), 100 Hz (red), 1 kHz (blue), 5 kHz (green), and 10 kHz (pink) with amplitude of 5 V (Figure 5b). The formation of lipid nanotubes for each given amplitude and frequency was carried out at least three times. The length of the lipid nanotube was calculated from at least 20 randomly selected data for each dot. It is noted that the lipid nanotubes grow up with different speed, but they all grow faster in an earlier stage and reach maximum length at a certain point. The maximum length of lipid nanotubes increases gradually from 1 to 5 V and decreases with increasing frequency. The maximum length can be up to about 200 μm at an amplitude of 5 V and a frequency of 10 Hz. Electric field force, bending energy, and elastic force of lipids are the main factors for the lipid nanotube electroformation. Lateral electric field force increases with the amplitude of the AC electric field increasing,[41] causing longer nanotubes in electric field from 1 to 5 V (Figure 5a). On the contrary, the higher frequency leads to the shorter time for electric field force to drive the growth of lipid nanotubes in one period, consequently resulting in shorter lipid nanotube formation (Figure 5b). The elastic force and bilayer bending energy are two factors for hindering lipid nanotube growth. When the electric field force is equal to the sum of bending force and elastic force, the length of the lipid nanotube reaches the maximum. The length of these lipid nanotubes is on the same order of magnitude as those formed by stretching.[23,34]

On the basis of experimental results in Figure 5, we proposed below an equation to describe the relationship of growth length of lipid nanotube (L) against time (t):

$$L = L_\infty(1 - e^{-t/\tau}) \quad (5)$$

where L_∞ is the maximum length of the lipid nanotube and τ^{-1} is apparent rate constant of lipid nanotube growth. As mentioned before, the lipid nanotube growth is governed by the electric field force, bending energy, and elastic force. Therefore, L_∞ was deduced and given below. The detailed deduction process is presented in the section of "formula deduction" of Supporting Information.

$$L_\infty = \frac{\frac{\pi {R_{opt}}^2}{3}\varepsilon_m f_{cm}\left(\frac{dV}{dx}\right)^2 - \frac{2\pi k_c}{R_{opt}}}{\gamma_0} \quad (6)$$

By bring eq 6 into eq 5, the below equation is obtained.

$$L = \frac{\frac{\pi {R_{opt}}^2}{3}\varepsilon_m f_{cm}\left(\frac{dV}{dx}\right)^2 - \frac{2\pi k_c}{R_{opt}}}{\gamma_0}(1 - e^{-t/\tau}) \quad (7)$$

where dV/dx is electric field strength, ε_m is medium permittivity, f_{cm} is the real part of Clausius–Mossotti

(CM) factor, γ_0 (related with elastic energy) is lipid membrane tension at the maximum length of lipid nanotubes, k_c is 74.5 pN nm, and R_{opt} is 265 nm. The relationship among f_{cm}, ε_m, and frequency f is provided in Supporting Information Figure S3. The total expression of $(\pi R_{opt}^2/3)\varepsilon_m f_{cm}(dV/dx)^2$ is the electric field force exerted on the lipid nanotube in the AC electric field; $(2\pi k_c)/R_{opt}$ is responsible for bending energy. From eq 7, it shows that the length of lipid nanotube is influenced by AC electric field parameters (*i.e.*, amplitude and frequency). Using eq 7 to fit experimental data in Figure 5 (solid lines), we obtained γ_0 to be 3.4×10^{-4} pN nm^{-1}, which is consistent with reported values,[42,43] which together with the exellent matching of fitting curves with experimental data confirm the validity of eq 7 to describe the lipid growing process. Value of τ^{-1} was obtained to be 0.051, 0.084, and 0.103 min^{-1} at amplitudes of 1, 3, and 5 V, respectively, with a frequency of 10 Hz, and 0.098, 0.074, 0.043, and 0.033 min^{-1} at frequencies of 100 Hz, 1 kHz, 5 kHz, and 10 kHz, respectively, with an amplitude of 5 V. The larger τ^{-1} value indicates faster lipid nanotube growth.

Silica Mineralization on Lipid Nanotubes. To explore the application of the formed lipid nanotube, we used them as templates for silica mineralization. Tetraethylorthosilicate (TEOS) was used as silicon source materials to mineralize the formed lipid nanotubes at pH 5. Scanning electron microscopy (SEM) of silica-coated lipid nanotubes is shown in Figure 6. From the image of a broken nanotube (inset image), it is noted that the silica-coated lipid nanotube remains hollow inside. The silica film on the nanotube surface remained continuous after extensive washing with water, indicating a strong adherence of the silica film to the nanotube surface. Due to the excellent biocompatibility of silica, silica-mineralized nanotubes have great potential in many fields, such as biomolecular recognition for specific proteins, single-DNA sensing, bioseparations, gene delivery, and controlled drug delivery.[44−46] In addition to be templates for silica metallization, lipid nanotubes are the versatile channel models to investigate the material delivery between cells *in vitro*. They may also find applications on microreactors for DNA transcription and on nanofluidics due to their channel size.

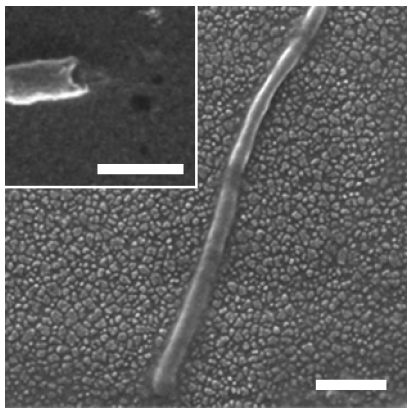

Figure 6. SEM image of silica-mineralized lipid nanotube. The inset is a broken nanotube. The scale bar is 1 μm.

CONCLUSIONS

In summary, the electric field distribution from coplanar interdigitated electrodes can be regulated by solution height above the electrodes. This phenomenon was successfully explored to generate lipid nanotubes. At low enough solution height, lateral electric field components generate the main driving force of nanotube growth along with the electric field direction, and an equation was obtained to describe the relationship among nanotube length and field frequency, amplitude, and time. The formation mechanism was proposed based on both experimental and simulated results. The internal lipid fluidity is as good as that in other model cell membrane system, which allows them to be used as a model system in biology studies. The nanotube length can be well-controlled, which makes the nanotube a good template for nanowire fabrication. This lipid nanotube forming method is easy and flexible and has great potential both in biology and nanotechnology fields. More importantly, the presented approach opens a way to design and prepare nanoscale materials with unique structural properties using space-regulated electric fields.

MATERIALS AND METHODS

Lipid Solutions. L-α-Phosphatidylcholine from egg yolk (egg PC) and chloroform were purchased from Sigma (China). 1,2-Dioleoyl-*sn*-glycero-3-phosphocholine (DOPC), Texas red-labeled 1,2-dihexadecanoyl-*sn*-glycero-3-phosphoethanolamine, triethylammonium salt (TR-DHPE), and fluorescence-labeled 1,2-dioleoyl-*sn*-glycero-3-phosphoethanolamine-*N*-(7-nitro-2-1,3-benzoxadiazol-4-yl) (NBD PE were purchased from Avanti Polar Lipids (USA). Lipid solutions of egg PC (10.0 mg mL^{-1}, doped with 2% NBD PE or 0.5%TR-DHPE, mass ratio) and DOPC (doped with 0.5% TR-DHPE, mass ratio) were prepared in chloroform. At such low concentration of fluorescent lipids, their effect on the mechanical properties of the membrane is known to be negligible.[47]

Lipid Nanotube Formation and Measurement. Five microliter lipid solutions were deposited onto an interdigitated ITO electrode surface using a needle to spread carefully back and forth five times. Uniform lipid films were then obtained by drying under vacuum for 2 h. A certain volume of deionized water was gently dropped into the slot on the electrode surface and then a coverslip placed on top of it. A sinusoidal AC electric field was applied to induce lipid nanotube formation. Lipid nanotube formation was observed under a fluorescence microscope (Nikon 80i, Japan).

Finite Element Analysis of Electric Field Distribution with COMSOL Software. The electric field distribution is simulated using the AC/DC module of COMSOL Multiphysics 4.3. The vector equation of electric potential in homogeneous medium can be

written as the Laplace equation:

$$\nabla \cdot [(\sigma + i\omega\varepsilon)\nabla\tilde{\varphi}] = 0 \quad (8)$$

where σ is the electric conductivity, ε is the permittivity, ω is angular frequency, and φ is electric potential. Dirichlet boundary condition was applied on electrodes (*i.e.*, $V = \pm V_0$). Von Neuman boundary condition was applied for top and bottom boundaries in order to mathematically separate the conductive segment from its surroundings (*i.e.*, $\partial\varphi/\partial n = 0$). Left and right boundaries were set as periodic boundary conditions. A sheet above the electrodes was set to represent thin lipid film during the simulation, where the resistance value was obtained from the experimental measurement using electrochemical impedance spectroscopy (Supporting Information Figure S4). The thickness of the sheet was also obtained from actual measurement using atomic force microscopy (Supporting Information Figure S5). The simulation was finished with a triangular grid meshing. The mesh was adjusted according to local structure to obtain the required convergence at a reasonable computing time scale while maintaining the required accuracy. There were 8.0×10^4 to 1.0×10^5 triangular elements involved in the simulation. The input parameters are listed in Supporting Information Table S1.

Silica Mineralization on Lipid Nanotubes. After lipid nanotube electroformation, the whole chamber was placed into a small container filled with water, and then the top coverslip and spacer were carefully removed. By shaking the solution gently, lipid nanotubes detached from the electrodes and were suspended in the water. TEOS was added to the gently shaked lipid nanotube suspension (pH 5, molar ratio TEOS/lipid = 120:1), then kept for 20 days at room temperature. The samples were washed three times with deionized water and metalized with gold by sputter coating prior to scanning electron microscopy (FEI Quanta 200F).

Conflict of Interest: The authors declare no competing financial interest.

Acknowledgment. We thank the National Natural Science Foundation of China (Nos. 21273059 and 21003032) and Open Research Fund of the State Key Laboratory of Electroanalytical Chemistry (Grant No. SKLEAC201313) for financial support.

Supporting Information Available: Figures S1–S5, Table S1, movie S1, and formula deduction are provided in the Supporting Information. This material is available free of charge *via* the Internet at http://pubs.acs.org.

REFERENCES AND NOTES

1. Karlsson, A.; Karlsson, R.; Karlsson, M.; Cans, A. S.; Stromberg, A.; Ryttsen, F.; Orwar, O. Molecular Engineering—Networks of Nanotubes and Containers. *Nature* **2001**, *409*, 150–152.
2. Rustom, A.; Saffrich, R.; Markovic, I.; Walther, P.; Gerdes, H. H. Nanotubular Highways for Intercellular Organelle Transport. *Science* **2004**, *303*, 1007–1010.
3. Schnur, J. M. Lipid Tubules—A Paradigm for Molecularly Engineered Structures. *Science* **1993**, *262*, 1669–1676.
4. Stinchcombe, J. C.; Bossi, G.; Booth, S.; Griffiths, G. M. The Immunological Synapse of CTL Contains a Secretory Domain and Membrane Bridges. *Immunity* **2001**, *15*, 751–761.
5. Liu, H. Q.; Bachand, G. D.; Kim, H.; Hayden, C. C.; Abate, E. A.; Sasaki, D. Y. Lipid Nanotube Formation from Streptavidin–Membrane Binding. *Langmuir* **2008**, *24*, 3686–3689.
6. Tanaka, M.; Critchley, K.; Matsunaga, T.; Evans, S. D.; Staniland, S. S. Fabrication of Lipid Tubules with Embedded Quantum Dots by Membrane Tubulation Protein. *Small* **2012**, *10*, 1590–1595.
7. Nakashima, N.; Asakuma, S.; Kunitake, T. Optical Microscopic Study of Helical Superstructures of Chiral Bilayer-Membranes. *J. Am. Chem. Soc.* **1985**, *107*, 509–510.
8. Dubey, G. P.; Ben-Yehuda, S. Intercellular Nanotubes Mediate Bacterial Communication. *Cell* **2011**, *144*, 590–600.
9. Georger, J. H.; Singh, A.; Price, R. R.; Schnur, J. M.; Yager, P.; Schoen, P. E. Helical and Tubular Microstructures Formed by Polymerizable Phosphatidylcholines. *J. Am. Chem. Soc.* **1987**, *109*, 6169–6175.
10. Baral, S.; Schoen, P. Silica-Deposited Phospholipid Tubules as a Precursor to Hollow Submicron-Diameter Silica Cylinders. *Chem. Mater.* **1993**, *5*, 145–147.
11. Patil, A. J.; Muthusamy, E.; Seddon, A. M.; Mann, S. Higher-Order Synthesis of Organoclay Pipes Using Self-Assembled Lipid Templates. *Adv. Mater.* **2003**, *15*, 1816–1819.
12. Zhou, Y.; Shimizu, T. Lipid Nanotubes: A Unique Template To Create Diverse One-Dimensional Nanostructures. *Chem. Mater.* **2008**, *20*, 625–633.
13. Yang, B.; Kamiya, S.; Shimizu, Y.; Koshizaki, N.; Shimizu, T. Glycolipid Nanotube Hollow Cylinders as Substrates: Fabrication of One-Dimensional Metallic-Organic Nanocomposites and Metal Nanowires. *Chem. Mater.* **2004**, *16*, 2826–2831.
14. Shimizu, T. Self-Assembled Lipid Nanotube Hosts: The Dimension Control for Encapsulation of Nanometer-Scale Guest Substances. *J. Polym. Sci., Part A: Polym. Chem.* **2006**, *44*, 5137–5152.
15. Zhou, Y.; Kogiso, M.; He, C.; Shimizu, Y.; Koshizaki, N.; Shimizu, T. Fluorescent Nanotubes Consisting of CdS-Embedded Bilayer Membranes of a Peptide Lipid. *Adv. Mater.* **2007**, *19*, 1055–1058.
16. Yager, P.; Schoen, P. E. Formation of Tubules by a Polymerizable Surfactan. *Mol. Cryst. Liq. Cryst.* **1984**, *106*, 3–4.
17. Yager, P.; Schoen, P. E.; Davies, C.; Price, R.; Singh, A. Structure of Lipid Tubules Formed from a Polymerizable Lecihin. *Biophys. J.* **1985**, *48*, 899–906.
18. Chappell, J. S.; Yager, P. Formation of Mineral Microstructures with a High Aspect Ratio from Phospholipid-Bilayer Tubules. *J. Mater. Sci. Lett.* **1992**, *11*, 633–636.
19. Burke, T. G.; Rudolph, A. S.; Price, R. R.; Sheridan, J. P.; Dalziel, A. W.; Singh, A.; Schoen, P. E. Differential Scanning Calorimetric Study of the Thermotropic Phase-Behavior of a Polymerizable, Tubule-Forming Lipid. *Chem. Phys. Lipids* **1988**, *48*, 215–230.
20. Itojima, Y.; Ogawa, Y.; Tsuno, K.; Handa, N.; Yanagawa, H. Spontaneous Formation of Helical Structures from Phospholipid-Nucleoside Conjugates. *Biochemistry* **1992**, *31*, 4757–4765.
21. Pescador, P.; Brodersen, N.; Scheidt, H. A.; Loew, M.; Holland, G.; Bannert, N.; Liebscher, J.; Herrmann, A.; Huster, D.; Arbuzova, A. Microtubes Self-Assembled from a Cholesterol-Modified Nucleoside. *Chem. Commun.* **2010**, *46*, 5358–5360.
22. Sugihara, K.; Chami, M.; Derenyi, I.; Voros, J.; Zambelli, T. Directed Self-Assembly of Lipid Nanotubes from Inverted Hexagonal Structures. *ACS Nano* **2012**, *6*, 6626–6632.
23. Sekine, Y.; Abe, K.; Shimizu, A.; Sasaki, Y.; Sawada, S.; Akiyoshi, K. Shear Flow-Induced Nanotubulation of Surface-Immobilized Liposomes. *RSC Adv.* **2012**, *2*, 2682–2684.
24. Rossier, O.; Cuvelier, D.; Borghi, N.; Puech, P. H.; Derenyi, I.; Buguin, A.; Nassoy, P.; Brochard-Wyart, F. Giant Vesicles under Flows: Extrusion and Retraction of Tubes. *Langmuir* **2003**, *19*, 575–584.
25. Evans, E.; Bowman, H.; Leung, A.; Needham, D.; Tirrell, D. Biomembrane Templates for Nanoscale Conduits and Networks. *Science* **1996**, *273*, 933–935.
26. Borghi, N.; Brochard-Wyart, F. Tether Extrusion from Red Blood Cells: Integral Proteins Unbinding from Cytoskeleton. *Biophys. J.* **2007**, *93*, 1369–1379.
27. Pascoal, P.; Kosanic, D.; Gjoni, M.; Vogel, H. Membrane Nanotubes Drawn by Optical Tweezers Transmit Electrical Signals between Mammalian Cells over Long Distances. *Lab Chip* **2010**, *10*, 2235–2241.
28. Avouris, P.; Chen, Z. H.; Perebeinos, V. Carbon-Based Electronics. *Nat. Nanotechnol.* **2007**, *2*, 605–615.
29. Freer, E. M.; Grachev, O.; Duan, X.; Martin, S.; Stumbo, D. P. High-Yield Self-Limiting Single-Nanowire Assembly with Dielectrophoresis. *Nat. Nanotechnol.* **2010**, *5*, 525–530.
30. Smith, P. A.; Nordquist, C. D.; Jackson, T. N.; Mayer, T. S.; Martin, B. R.; Mbindyo, J.; Mallouk, T. E. Electric-Field

Assisted Assembly and Alignment of Metallic Nanowires. *Appl. Phys. Lett.* **2000**, *77*, 1399–1401.
31. Angelova, M. I.; Dimitrov, D. S. Liposome Electroformation. *Faraday Discuss.* **1986**, *81*, 303–311.
32. Okumura, Y.; Zhang, H.; Sugiyama, T.; Iwata, Y. Electroformation of Giant Vesicles on a Non-electroconductive Substrate. *J. Am. Chem. Soc.* **2007**, *129*, 1490–1491.
33. Bi, H.; Yang, B.; Wang, L.; Cao, W.; Han, X. Electroformation of Giant Unilamellar Vesicles Using Interdigitated ITO Electrodes. *J. Mater. Chem. A* **2013**, *1*, 7125–7130.
34. Brazhnik, K. P.; Vreeland, W. N.; Hutchison, J. B.; Kishore, R.; Wells, J.; Helmerson, K.; Locascio, L. E. Directed Growth of Pure Phosphatidylcholine Nanotubes in Microfluidic Channels. *Langmuir* **2005**, *21*, 10814–10817.
35. Douliez, J. P.; Pontoire, B.; Gaillard, C. Lipid Tubes with a Temperature-Tunable Diameter. *ChemPhysChem* **2006**, *7*, 2071–2073.
36. Chen, Z.; Rand, R. P. The Influence of Cholesterol on Phospholipid Membrane Curvature and Bending Elasticity. *Biophys. J.* **1997**, *73*, 267–276.
37. Kozlov, M. M.; Leikin, S.; Rand, R. P. Bending, Hydration and Interstitial Energies Quantitatively Account for the Hexagonal-Lamellar-Hexagonal Reentrant Phase-Transition in Dioleoylphosphatidylethanolamine. *Biophys. J.* **1994**, *67*, 1603–1611.
38. Soumpasis, D. M. Theoretical Analysis of Fluorescence Photobleaching Recovery Experiments. *Biophys. J.* **1983**, *41*, 95–97.
39. Han, X. J.; Qi, G. D.; Xu, X. T.; Wang, L. Formation of Lipid Bilayer Microarrays on Photo-oxidized Polystyrene Surfaces. *Chem.—Eur. J.* **2011**, *17*, 14741–14744.
40. Stelzle, M.; Miehlich, R.; Sackmann, E. Two-Dimensional Microelectrophoresis in Supported Lipid Bilayers. *Biophys. J.* **1992**, *63*, 1346–1354.
41. Dimitrov, D. S.; Angelova, M. I. Lipid Swelling and Liposome Formation on Solid Surfaces in External Electric Fields. *Prog. Colloid Polym. Sci.* **1987**, 48–56.
42. Fa, N.; Lins, L.; Courtoy, P. J.; Dufrene, Y.; Van Der Smissen, P.; Brasseur, R.; Tyteca, D.; Mingeot-Leclercq, M. P. Decrease of Elastic Moduli of DOPC Bilayers Induced by a Macrolide Antibiotic, Azithromycin. *Biochim. Biophys. Acta* **2007**, *1768*, 1830–1838.
43. Castillo, J. A.; Narciso, D. M.; Hayes, M. A. Bionanotubule Formation from Surface-Attached Liposomes Using Electric Fields. *Langmuir* **2009**, *25*, 391–396.
44. Fan, R.; Karnik, R.; Yue, M.; Li, D. Y.; Majumdar, A.; Yang, P. D. DNA Translocation in Inorganic Nanotubes. *Nano Lett.* **2005**, *5*, 1633–1637.
45. Chen, C. C.; Liu, Y. C.; Wu, C. H.; Yeh, C. C.; Su, M. T.; Wu, Y. C. Preparation of Fluorescent Silica Nanotubes and Their Application in Gene Delivery. *Adv. Mater.* **2005**, *17*, 404–407.
46. Mitchell, D. T.; Lee, S. B.; Trofin, L.; Li, N. C.; Nevanen, T. K.; Soderlund, H.; Martin, C. R. Smart Nanotubes for Bioseparations and Biocatalysis. *J. Am. Chem. Soc.* **2002**, *124*, 11864–11865.
47. Bouvrais, H.; Pott, T.; Bagatolli, L. A.; Ipsen, J. H.; Méléard, P. Impact of Membrane-Anchored Fluorescent Probes on the Mechanical Properties of Lipid Bilayers. *Biochim. Biophys. Acta* **2010**, *1798*, 1333–1337.